Available online at www.sciencedirect.com
ScienceDirect
Earth and Planetary Science Letters 262 (2007) 398–412
EPSL
www.elsevier.com/locate/epsl

Low S velocity atop the 410-km discontinuity and mantle plumes

L. Vinnik [a,*], V. Farra [b]

[a] Institute of physics of the Earth, B. Grouzinskaya, 10, 123995, Moscow, Russia
[b] Institut de Physique du Globe de Paris, 4 Place Jussieu, F-75252 Paris cedex 05, France

Received 12 January 2007; received in revised form 13 July 2007; accepted 24 July 2007
Available online 9 August 2007
Editor: R.D. van der Hilst

Abstract

A thin, low-S-velocity layer atop the 410-km discontinuity is an intriguing feature of the upper mantle with important implications for geodynamics, but relevant seismic data are few. By applying S receiver function technique to more than 50 globally distributed stations, in 10 regions we obtain evidence for a negative discontinuity at a depth of about 350 km. In most cases, the low velocity is found beneath Precambrian platforms, in association with either Mesozoic or Cenozoic mantle plumes. This relationship suggests dehydration of water-bearing silicates as a possible reason for the low velocity, but contradicts the predictions of the transition-zone-water-filter model of Bercovici and Karato (Nature 425, 39-44, 2003). The presence of the low velocity beneath some Mesozoic traps, in spite of plate motions, implies the possibility of coupling of the continental lithosphere and the underlying upper mantle up to a depth of ~400 km.

Keywords: S receiver function; 410-km discontinuity; mantle plume; mantle transition zone; water-filter model

1. Introduction

In seismic models of the oceans and some continental regions, a low-S-velocity zone (LVZ) is present in a depth range of ca. 80–250 km. In this depth range the temperature is close to the mantle solidus, and this explains the origin of the low S velocity. The LVZ, though less well pronounced, is found at these depths beneath some old continental platforms. Another low velocity layer, several tens of kilometers thick is found atop the 410-km mantle discontinuity at a few locations beneath continents: east China (Revenaugh and Sipkin, 1994), the Kaapvaal (Vinnik et al., 1996b; Vinnik and Farra, 2002) and Siberian (Vinnik and Farra, 2002) cratons, Afar (Chevrot et al., 1999), the Arabian plate (Vinnik et al., 2003) and the northwestern USA (Song et al., 2004). The low S velocity might be a by-product of the transition zone water filter (Bercovici and Karato, 2003), and the seismic observations can be used for testing the predictions of this hypothesis.

The data for east China (Revenaugh and Sipkin, 1994) were obtained from multiple ScS reverberations and explained by dehydration of subducting lithosphere in the neighboring subduction zone. The data for the northwestern USA (Song et al., 2004) were obtained from the refracted S waves of local earthquakes, and, as in China, attributed to dehydration of the subducted (Farallon) plate. Evidence for the low-velocity layer

* Corresponding author.
E-mail addresses: vinnik@ifz.ru (L. Vinnik), farra@ipgp.jussieu.fr (V. Farra).

0012-821X/$ - see front matter © 2007 Elsevier B.V. All rights reserved.
doi:10.1016/j.epsl.2007.07.051

beneath Afar was found using P receiver functions (Chevrot et al., 1999), but it was not confirmed by S receiver functions (Vinnik et al., 2004a). The data for the other regions were obtained by using S receiver functions and interpreted as effects of either Mesozoic (Kaapvaal and Siberian cratons) (Vinnik and Farra, 2002) or Cenozoic mantle plumes (Arabian plate) (Vinnik et al., 2003). Early indications of low velocity beneath the Kaapvaal craton were found in P receiver functions (Vinnik et al., 1996b).

Seismic Sp phases in the S receiver functions are sensitive to upper mantle discontinuities, and here we present new observations of the low velocity atop the 410-km discontinuity, made by applying S receiver function techniques to the recordings of several tens of globally distributed seismograph stations (Fig. 1). At some stations the receiver functions were obtained for two or even three azimuthal sectors. At a number of stations the recordings were noisy, or other reasons made the data inconclusive. These stations are not shown in Fig. 1. Beyond the permanent stations in Fig. 1, the available database includes S receiver functions for several networks: the short-term MOMA array in the eastern USA (Vinnik et al., 2005a), the short-term GHENGIS and long-term KNET networks in the Tien Shan (Oreshin et al., 2002), three networks in Iceland (Vinnik et al., 2005b), a short-term network of several stations in Arabia (Vinnik et al., 2003) and two short-term stations in Afar (Vinnik and Farra, 2006). Our paper reports indications of the low S velocity atop the 410-km discontinuity at several new locations, which roughly doubles the number of locations known from previous studies.

Observations at station BOSA in southern Africa and NRIL in Siberia were presented in Vinnik and Farra (2002), but important details of the observations at NRIL were omitted for brevity. Here we describe them in detail. The other data are new. Previously published data for the Arabian plate (Vinnik et al., 2003) were based on recordings made at an array of short-term stations, and the detected signal was weak. Station RAYN of this group is permanent, and now we analyze a large data set from this station, practically independent of the data in Vinnik et al. (2003). The other data are based on the observations in Antarctica, several stations in east Asia, ARU in the Urals and TAM in northern Africa. Maps of these regions are displayed in Fig. 2. In east Asia, indications of a low S velocity over the 410-km discontinuity were found earlier in recordings of multiple ScS reverberations (Revenaugh and Sipkin, 1994), but the wave paths from the 410-km discontinuity to the receiver in the S receiver functions are very short in comparison with those of ScS reverberations and the periods are about half as long. As a result, the first Fresnel zone of the Sp phases is an order of magnitude smaller than those of the ScS reverberations,

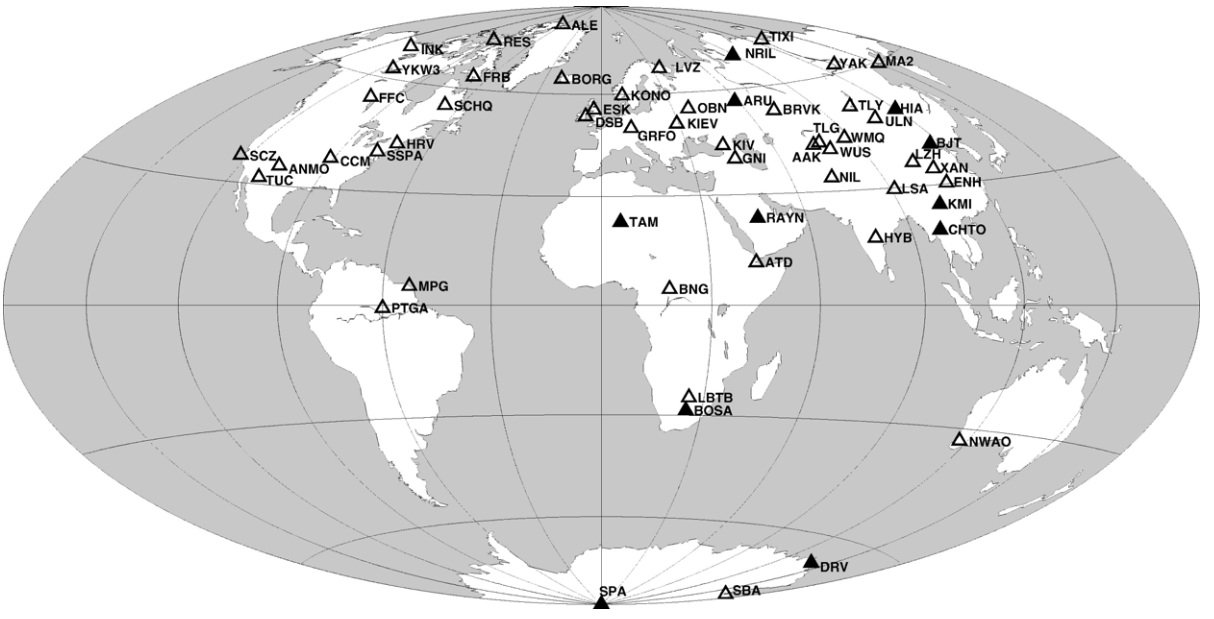

Fig. 1. Seismograph stations with and without indications of a low-S-velocity layer atop the 410-km discontinuity (filled and open triangles, respectively).

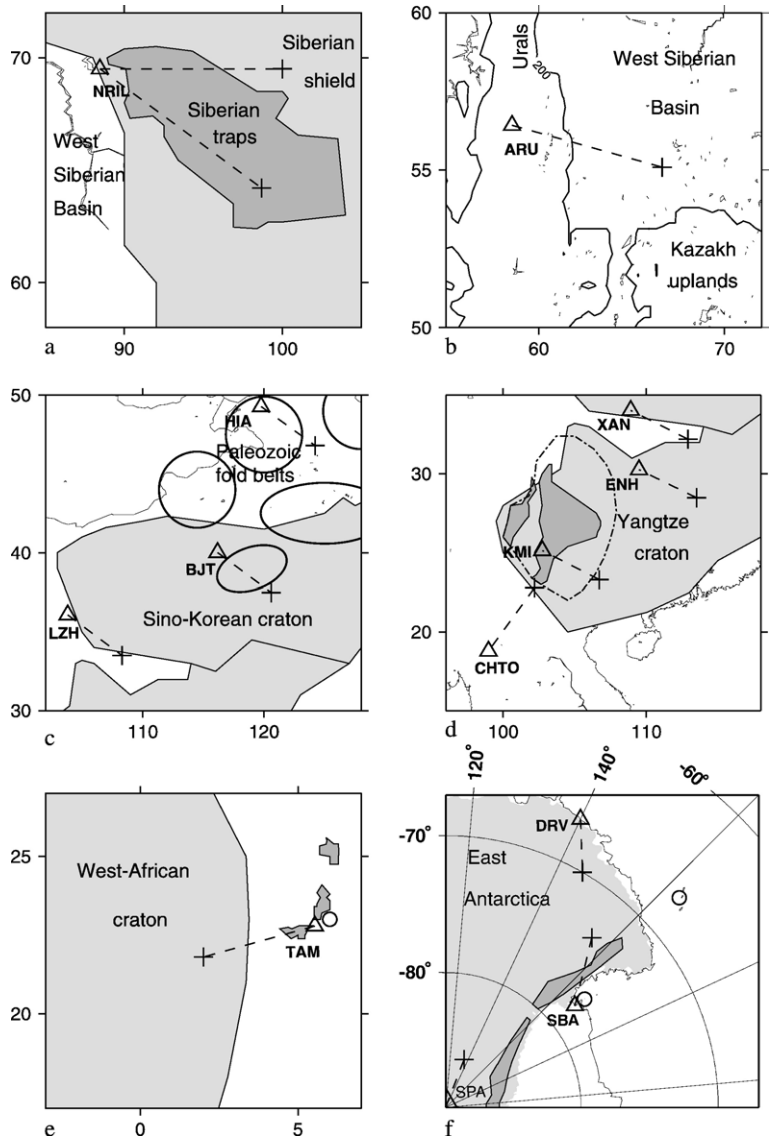

Fig. 2. Regions with low S velocity atop the 410-km discontinuity. Seismograph stations and the corresponding projections of the piercing points of the Sp phase at a depth of 350 km are shown by triangles and crosses, respectively; light shading indicates cratons; a) North Siberia; b) West Siberia, topography is shown by 200-m contour; c) Northeastern China with elements of tectonics (Zhang et al., 1984) and volcanic regions (Deng et al., 2004) (contoured by ellipses); d) Southeast Asia, dark shading indicates Emeishan traps; uplift preceding emplacement of the traps (He et al., 2003) is contoured by dot-dash line; e) North Africa, dark shading indicates Cenozoic volcanism; circle is for Hoggar hotspot (Duncan and Richards, 1991); f) Antarctica with hotspots (Duncan and Richards, 1991) (open circles); dark shading indicates Ferrar basalts (Heinmann et al., 1995).

and lateral resolution of our results is higher by about an order of magnitude.

2. The S receiver function technique

The S receiver function (SRF) is the response of the Earth in the vicinity of the seismograph station to the excitation by incoming S waves from distant earthquake (Farra and Vinnik, 2000). This response consists largely of Sp converted phases. The time advance of the converted phase relative to the parent S wave is sensitive to depth of the discontinuity, whereas the amplitude is nearly proportional to the S velocity contrast at the discontinuity. Amplitudes of the Sp converted phases from discontinuities in the mantle are a few percent in amplitude of the parent S, and special signal processing procedures are required to extract them from noise.

SRFs have much in common with the well-known P receiver functions that contain Ps converted phases, but in P receiver functions, the converted Ps phases from

discontinuities in the mantle arrive in the time interval dominated by multiple reflections and scattering from crustal discontinuities. In SRFs the mantle Sp phases arrive much earlier than crustal reverberations, which is an important advantage over P receiver functions. Moreover, some boundaries in the mantle are probably gradational. A gradational boundary with a thickness of ca. 30 km may be transparent at short periods in P receiver functions (2–5 s) but detectable at longer periods (10–15 s) in SRFs.

The central idea of the receiver function approach is detection of weak secondary signals by combined analysis of recordings of many seismic events recorded at the same seismograph station. A straightforward analysis of many recordings is hampered by differences between the individual waveforms radiated from different earthquakes. The individual S waveform can be represented by convolution of a standard delta-like pulse with the individual source function. Then the standard pulse can be retrieved by deconvolution. The deconvolution equalizes the secondary seismic phases such as Sp, and they can be detected by stacking many recordings. Assuming a similar level of noise in individual receiver functions, the signal/noise ratio in the stack is proportional to the square root of the number of recordings. In our study deconvolution is performed in time domain (Berkhout, 1977) with a proper regularization constant (usually, around 3.0).

To calculate SRF, the three-component recording is decomposed into the P, SV, T and M components (Farra and Vinnik, 2000). The SV axis corresponds to the principal S-particle-motion direction in the wave-propagation plane. The P axis is perpendicular to the SV in the same plane and is optimal for detecting Sp converted phases. The T (transverse) axis is perpendicular to SV and P. The M axis corresponds to the principal motion direction of the S wave in the T-SV plane, and is characterized by the angle θ with the SV axis. This angle is controlled by the focal mechanism of a seismic event. The P components are deconvolved by their respective M components. The converted phases can be generated by the SV and SH components of the incoming S. Combined processing of the deconvolved P components of many seismic events yields the response of the P component to the incoming SV component. The amplitude of this response is normalized to the SV component recorded at Earth's surface. The solution is equivalent to stacking the deconvolved P components of many recordings with weights depending on their respective θ and variance of noise. The procedure of record processing involves evaluation of σ, the RMS value of the random noise in the stack in the time interval from about −60 s to −20 s. The estimate of σ is obtained from the estimates of variance of the deconvolved P component amplitude of each record. We assume that this variance is determined only by noise, although a small fraction of it may be caused by the signals. The 95% confidence level corresponds to $\pm 2\sigma$ and we rate an arrival as a signal if its peak amplitude is at least 4 times σ. The actual signal amplitudes and values of σ are given in Table 1.

Table 1
Seismograph station codes, their coordinates (Lat and Lon), number of stacked individual receiver functions (Num), mean epicentral distance (Dist), mean back azimuth (Baz), RMS value of noise (σ), amplitude of the Sp phase from the 350 (km) discontinuity (Signal) and travel time delay of the Sp phase from the 350 (km) discontinuity relative to that from the 410 (km) discontinuity (time)

Sta	Lat	Lon	Num	Dist	Baz	σ	Signal	Time
	(degrees)	(degrees)		(degrees)	(degrees)			(s)
NRIL	69.50	88.44	81	75	147	0.008	0.033	7.2
NRIL	69.50	88.44	89	89	89	0.006		
ARU	56.43	58.56	201	79	106	0.004	0.016	8.8
BJT	40.02	116.17	81					
HIA	49.27	119.74	100					
HIA+BJT			181	82	128	0.004	0.019	10.7
LZH	36.09	103.84	63	79	118	0.006		
CHTO	18.81	98.94	39	78	37	0.013	0.055	7.3
KMI	25.12	102.74	105	82	116	0.004	0.016	7.8
ENH	30.27	109.49	162	81	122	0.004		
XAN	34.04	108.92	156	81	121	0.004		
RAYN	23.52	45.50	162	79	87	0.005	0.025	6.6
TAM	22.79	5.53	103	86	254	0.005	0.022	9.7
DRV	−66.67	140.01	76	83	148	0.006	0.025	7.1
SPA	−89.93	145.00	77	84	136	0.004	0.017	11.5
SBA	−77.85	166.76	199	77	330	0.003		

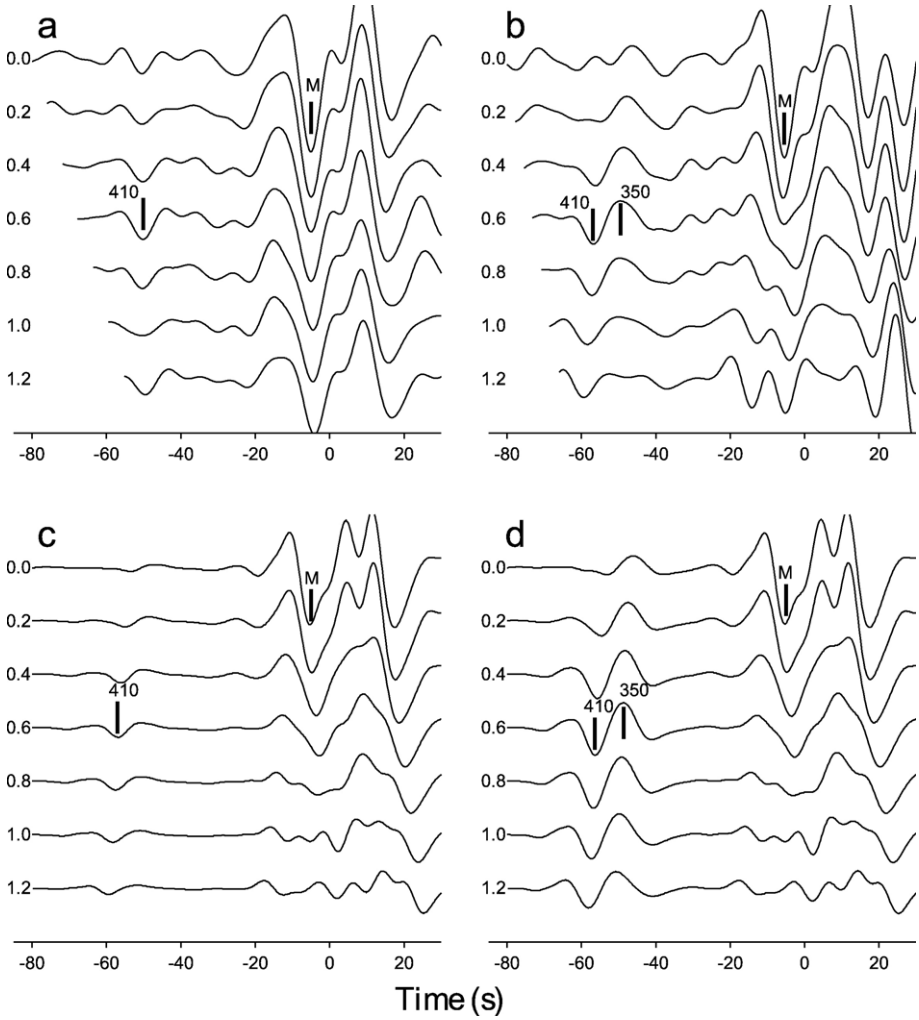

Fig. 3. P component of S receiver functions of station NRIL; numbers on the left are for differential slowness in s/°; origin of the time scale corresponds to the arrival of the S wave train. Note that the recordings of the P component do not contain the direct S wave. a) data for back azimuth of 89°, b) for back azimuth of 147°; c) synthetics for standard model (Kennett and Engdahl, 1991) in the back azimuth of 147°, d) synthetics for model in Fig. 5 in the back azimuth of 147°.

In addition to the signal/noise ratio, in the data there is a simple and robust indicator of quality of the SRF: a detection of the Sp phase from the global 410-km discontinuity implies that the method is sensitive enough to detect an S velocity contrast of about 0.2 km/s at a depth of about 400 km. Moreover, the greatest depth sampled by the SRF depends on epicentral distance. The Sp phase from a negative discontinuity becomes observable at a smaller epicentral distance than the Sp phase from a positive discontinuity at the same depth, and stacking in a broad distance range may result in a larger signal from the negative discontinuity.

The apparent velocity of the Sp converted phase from a deep discontinuity may be different from that of the parent phase. To account for this difference, the individual receiver functions are stacked with time delays (moveout corrections) depending on the assumed differential slowness (difference between the slowness of the Sp phase and the parent seismic phase). Seismic phases of interest are detected by inspecting the stack in a wide range of values of the differential slownesses. The theoretical differential slowness of the Sp phase from the 410-km discontinuity for a standard Earth's model is around 0.6 s/°, and almost the same slowness is expected for the phases converted between 300 and 400-km depths. The observed slowness (the slowness of the trace with the maximum amplitude of the signal) may deviate from the theoretical slowness owing to noise or lateral heterogeneity of the Earth: the differential

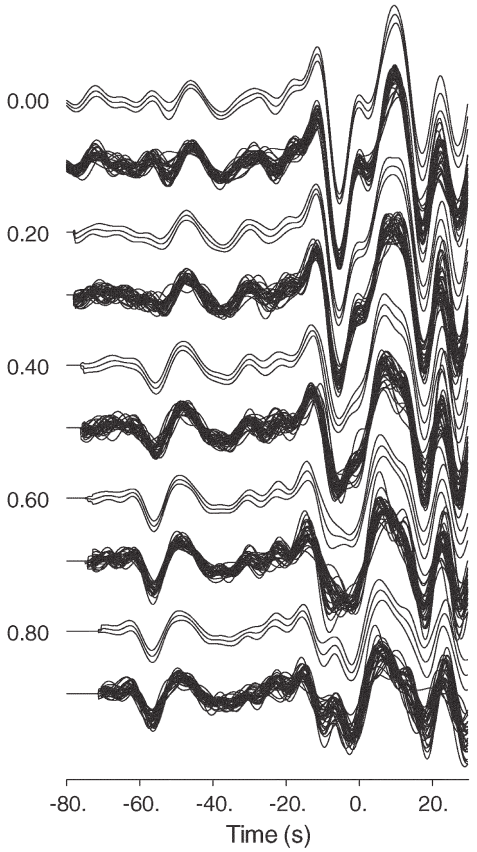

Fig. 4. Results of bootstrap resampling the individual receiver functions of station NRIL in the back azimuth of 147°. The stacks of the receiver functions (bottom) and the average with the $\pm\sigma$ interval (top) are shown for the differential slownesses from 0.0 to 0.8 s/° (numbers on the left).

slowness of the phase converted at a tilted boundary deviates from the standard value by about 0.2 s/° for a tilt of 1°.

The approximate position of the region sampled by the converted phase is determined by ray tracing for the Sp phase corresponding to the mean epicentral distance and back azimuth of the earthquakes. The piercing point thus determined is roughly at a similar distance from the seismograph station as the depth of the respective discontinuity. The shift is towards the epicenter (Fig. 2).

3. Analysis of the observations

We discuss the seismic data region by region. The individual receiver functions are from the epicentral distance range between 65° and 105°. The overwhelming majority of the earthquakes are closer than 90°. The width of each azimuthal sector is usually of the order of a few tens of degrees. The most important data parameters are presented in Table 1. Receiver functions of station NRIL and other results of data processing for this station are shown in Figs. 3, 4, 5. The receiver functions for the other stations, where the signal from the low-velocity layer is clear (signal/noise ratio not less than 4.0), are shown in Fig. 6. The other receiver functions are shown in Fig. 7.

The Sp phase from the 410-km discontinuity is very clear in all the receiver functions. This is a measure of the high quality of the data. Variations in time of this phase in the different data sets are caused partly by differences in the average epicentral distance (see Table 1). For every data set we calculated synthetic seismograms for standard model IASP91 (Kennett and Engdahl, 1991) and evaluated the difference in the arrival times of S410p between the actual data and the standard model. This difference, usually of the order of 1 s, is caused mainly by the different depth of the 410-km discontinuity and P and S velocities in the mantle above the 410-km discontinuity.

The weights used in the stacking procedure optimize the signal/noise ratio in the time interval −60 to −20 s. We do not interpret weak arrivals outside this window. Each seismic phase is seen on several traces in a certain range of differential slowness. We mark this arrival at the trace with the largest amplitude. The detected phases are labeled M (the Moho), L (the Lehmann discontinuity) or with the depth of the respective discontinuity in kilometers.

3.1. North Siberia, station NRIL

The recordings of station NRIL in north Siberia are in two azimuthal sectors with average back azimuths around 90° and 150° (Table 1 and Fig. 2a). The first

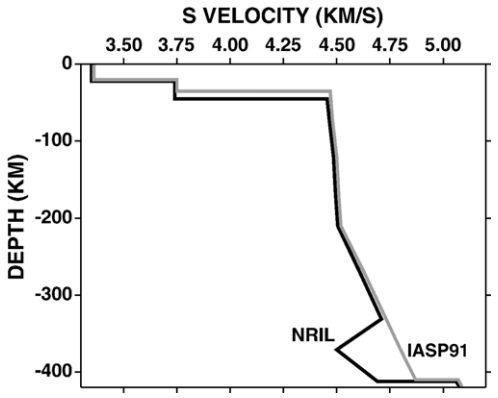

Fig. 5. S velocity model for the data of station NRIL in the back azimuth of 147°; S velocity for the standard model (Kennett and Engdahl, 1991) is shown for comparison.

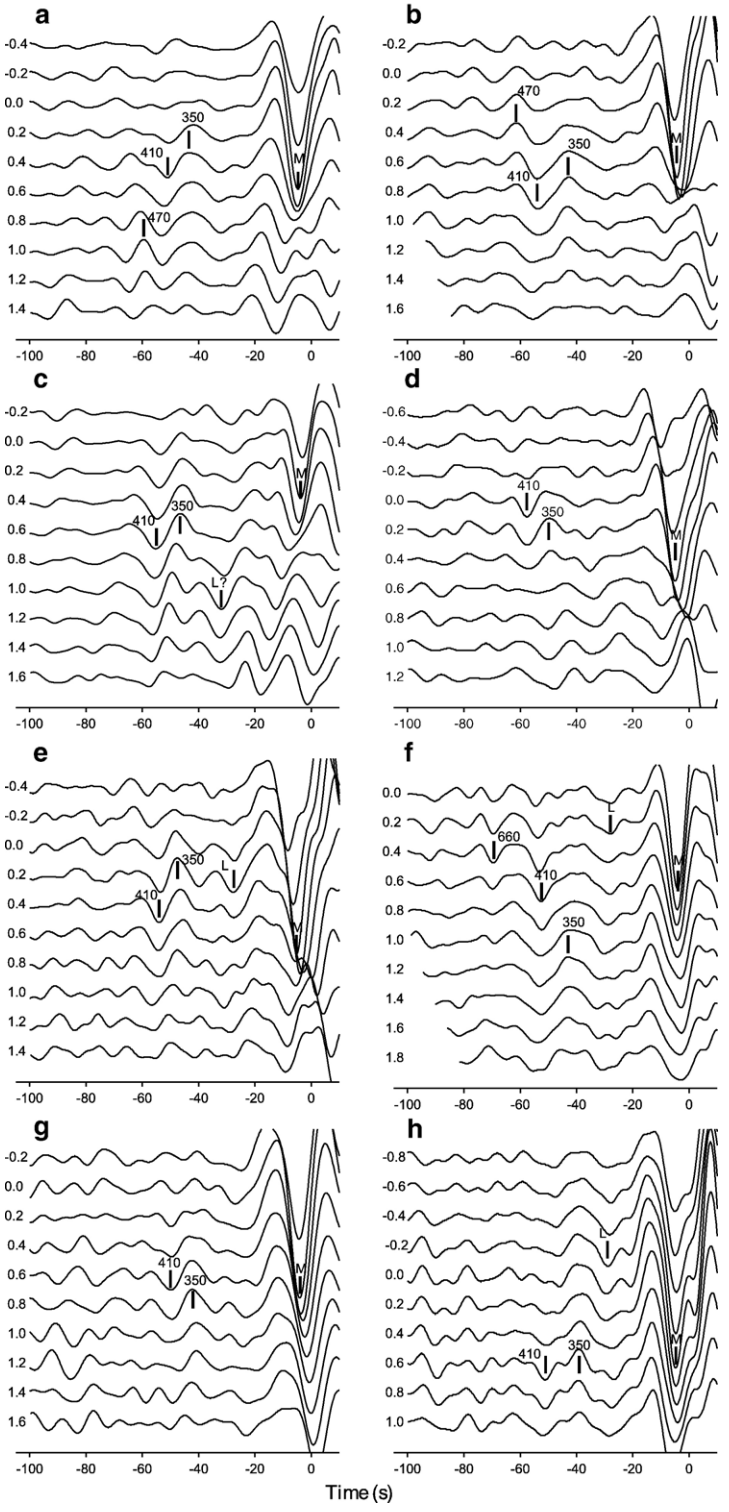

Fig. 6. The same as in Fig. 3b, but for the other stations with the large Sp phase from the 350-km discontinuity: a) ARU, b) HIA and BJT, c) CHTO, d) KMI, e) RAYN, f) TAM, g) DRV, h) SPA.

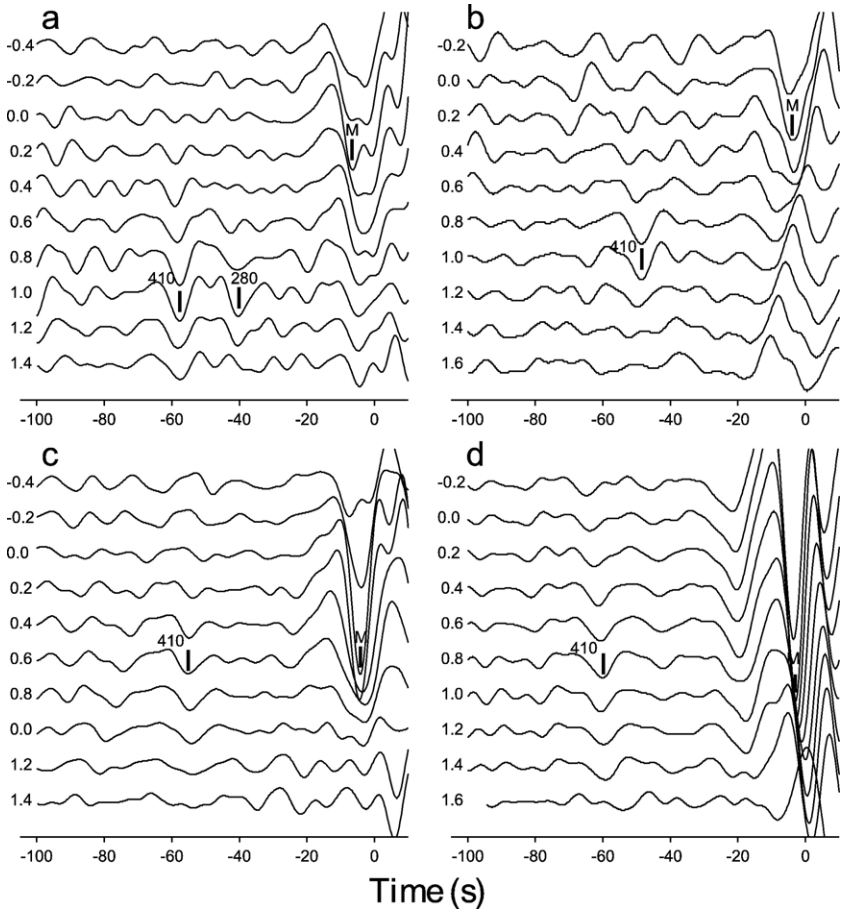

Fig. 7. The same as in Fig. 6, but for stations with either weak or missing Sp phase from the 350-km discontinuity: a) LZH, b) ENH, c) XAN, d) SBA.

stack is based on individual receiver functions in the sector between 0° and 125°. The data in the second stack are in the sector between 137° and 173°. Receiver functions for the first group contain Sp phases only from the Moho and the 410-km discontinuity (Fig. 3a). Negative polarity for both signals means that they are converted from positive discontinuities (with the higher S velocity at the lower side). The negative motion in the Sp phase from the Moho is preceded by a positive motion of a smaller amplitude. This positive motion is mainly a side lobe of the Sp phase from the Moho. The positive motion may contain the Sp phase from a negative discontinuity, separating the high-velocity mantle lid and the low-velocity zone beneath the lid at a depth of abound 100 km. To recognize this discontinuity, the data require an inversion (Oreshin et al., 2002; Vinnik et al., 2004b). The wave field in Fig. 3a can be viewed as standard, because it is typical for the great majority of stations shown in Fig. 1.

In the second azimuth the data are very different: the Sp phase from the 410-km discontinuity is followed by an arrival of about the same amplitude and opposite polarity (Fig. 3b). Its amplitude is 0.033, more than 4 times the RMS noise amplitude. The largest amplitude is at a time of −49.2 s at a differential slowness of 0.6 s/°, the standard value for the Sp phase converted at a depth of about 400 km in a spherically symmetrical Earth. Clear recording of the Sp phase from the 410-km discontinuity at a time of −56.4 s is an indication of the high quality of the data. The standard time for this arrival is −57.3 s.

Our estimates of the signal/noise ratio are based on the assumption that the level of noise in the time interval −60 to −20 s is independent of time. To test correctness of this assumption and of robustness of the observed signals, we conducted bootstrap resampling (Efron and Tibshirani, 1991) of the receiver functions in the second azimuth. The results (Fig. 4) indicate that the noise level σ is only weakly dependent on time and, for practical purposes, is similar to that in Table 1. Similar consistency of the estimates of σ was found for the recordings of other stations.

To construct the appropriate velocity model, we calculated synthetic S receiver functions with the reflectivity technique described in Vinnik et al. (2004), and searched for the preferred S velocity profiles by trial and error. The adopted input signal generates the deconvolved SV component, similar to that obtained in the actual data. The details of the models cannot be determined uniquely, but at this stage we are interested only in the approximate depth of the negative discontinuity and magnitude of the S velocity reduction. We assumed that the 410-km discontinuity is at its standard depth, and perturbed IASP91 standard model (Kennett and Engdahl, 1991) above the 410-km discontinuity, to obtain the model with the arrival times and amplitudes of the Sp phases from the negative discontinuity and the 410-km discontinuity, close to those in the actual receiver function. Synthetic receiver functions for the standard model (Kennett and Engdahl, 1991) do not contain the arrival with the positive polarity (Fig. 3c), but it is reproduced in the synthetics (Fig. 3d) for the model in Fig. 5. The S velocity in the layer over the 410-km discontinuity in this model is lowered by about 4% (0.2 km/s) relative to the standard, whereas the Vp/Vs ratio is unchanged. The upper boundary of the layer (negative discontinuity) is gradational, with its middle at 350-km depth. This boundary in the data of other stations will be labeled "350", although its actual depth in the other regions may vary in a range of about ±20 km. The period of the observed Sp phase from the negative discontinuity is relatively long, and the gradational discontinuity provides a low-pass filtering effect. The synthetics in Fig. 3 deviate from the actual receiver functions in the time interval 0–30 s. This interval in the receiver functions is formed by multiple crustal reflections, and in the context of our paper is only of cosmetic significance.

Our study region is part of the Siberian craton, of Archean age, and distinguished by traps (Fig. 2a) 250 Myr old and occupying more than 2.5 million square kilometers in the Tunguska depression (Zolutkhin and Al'mukhamedov, 1988). In the back azimuths corresponding to the data shown in Fig. 3a and b the Sp phases propagate at a depth of about 350 km either outside the traps or beneath them. As no other significant magmatic events are known in this region from the last 250 Myr, this distinction suggests that the low S velocity is a signature of the plume.

3.2. West Siberia, station ARU

Receiver functions of station ARU in the south Urals (Fig. 6a) are obtained by stacking large number (201) of individual receiver functions in the back azimuth sector 82°–134°. Beyond the standard Sp phases from the Moho and the 410-km discontinuity, the stack contains a long-period arrival with positive polarity at a time of about −43 s. Its amplitude (0.016) is 4 times the RMS amplitude of noise (0.004). The differential slowness of 0.4 s/° is close to the standard value of 0.6 s/°. We interpret this arrival as the Sp phase from the negative 350-km discontinuity. The piercing point of this phase is located beneath the margin of the West Siberian Basin (Fig. 2b). Evidence for this seismic phase is missing in the receiver functions of station BRVK in the Kazakh shield, 600 km to the east of station ARU. Another arrival with positive polarity is detected at a time of about −60 s. This may be the Sp phase from the top of a low velocity layer in the mantle transition zone (Vinnik and Farra, 2006).

The Urals mark the Paleozoic collision of the East European platform with the Altaids of Asia (Zonenshain et al., 1984). The tectonic evolution of the belt included rifting, initiation of island arcs in a paleo-ocean, its closure and continental collision. The region over the piercing point is a collage of island arc terranes and continental fragments (Sengor et al., 1993). The region to the northeast of the piercing point, the West Siberian Basin (WSB) of Mesozoic age, represents one of the largest sedimentary basins in the world. There are reasons to believe the WSB belongs to the same large igneous province as the Siberian traps (Reichow et al., 2002); the buried basalts of the WSB are of the same age as those in Siberian traps. However, the volume and extent of the WSB basalts are poorly known, owing to the thick sedimentary cover.

3.3. Northeast China, stations HIA, BJT and LZH

At stations HIA, BJT and LZH (Fig. 2c) we processed recordings in the back azimuth sector centered at about 125°. In the receiver functions of stations HIA and BJT there are similar details, and in order to detect them most reliably we processed jointly the data from both stations. In the resulting stack, beyond the standard signals from the Moho and the 410-km discontinuity, there are two arrivals with positive polarity preceding and following the 410-km converted phase (Fig. 6b). The former signal, which may correspond to the top of a low S velocity layer in the mantle transition zone was described in Vinnik and Farra (2006). Amplitude of the second signal is 0.019, almost 5 times the RMS noise amplitude. This is the Sp phase from the 350-km discontinuity. The largest amplitudes of both S350p and S410p are observed at a

slowness of 0.8 s/°. Both deviate in a similar way from the standard slowness of 0.6 s/°, which suggests that the deviations are caused mainly by lateral heterogeneity in the upper 350 km. The wave field at station LZH is very different and contains beyond the signals from the Moho and the 410-km discontinuity an arrival with negative polarity at a time around −40 s (Fig. 7a). This arrival corresponds to a positive discontinuity at a depth around 280 km.

Stations BJT and HIA and the related piercing points are located in northeastern China, which is characterized by thin lithosphere, rifting, high upper-mantle temperatures and numerous exposures of mostly Cenozoic basalts (Fig. 2c). These properties can be explained by mantle plumes (Deng et al., 2004). Station BJT and the region sampled by its data belong to the eastern Sino-Korean craton. Starting in the Jurassic, the Archean mantle lithosphere of the craton was replaced by denser, hotter rocks (Griffin et al., 1998). Evidence for a similar thermal agitation is missing for the western Sino-Korean craton sampled by the data from station LZH.

3.4. Southeast China, stations CHTO, KMI, ENH and XAN

The upper mantle of southeast Asia (Fig. 2d) is sampled by recording from stations CHTO, KMI, ENH and XAN. Most of the seismic events are in the southwest Pacific (at back azimuths of about 120°). There were too few recordings from the seismically active region to the northeast of the stations, with the exception of station CHTO. All receiver functions contain clear signals from the Moho and 410-km discontinuity. The receiver functions of station CHTO (Fig. 6c) contain an arrival with positive polarity, corresponding to the 350-km discontinuity. This arrival is observed at the standard slowness. Its amplitude is more than 4 times the RMS noise amplitude. At a time of about −30 s there is an arrival with negative polarity, which can be tentatively interpreted as the Sp phase from the positive Lehmann discontinuity at a depth of about 200 km, although the deviation of slowness of this phase (1.0 s/°) from the standard value (0.1 s/°) is very large.

The Sp phase with positive polarity is also visible in the data from station KMI (Fig. 6d). The signal/noise ratio for this arrival is nearly 4.0. The signal is focused at a differential slowness of 0.2 s/°, which deviates from the standard value. A qualitatively similar deviation is observed in the Sp phase from the 410-km discontinuity. Similar trends in both signals suggest that the effect is caused by lateral velocity heterogeneity at depths shallower than 350 km. In the receiver functions of stations ENH and XAN (Fig. 7b, c) the phase with positive polarity is either missing or the signal/noise ratio is too low for a robust detection.

The region sampled by this data group is outside the area of Cenozoic basaltic volcanism in the north. In the context of our study, the major features of the region, sampled by receiver functions from stations CHTO and KMI are the Yangtze craton and Emeishan traps (Fig. 2d). The craton is of the Archean age. The Emeishan traps erupted at about the same time as the Siberian traps (258 Myr) (Davaille et al., 2005). The mantle plume model fits the data available for the Emeishan flood basalts (Chang and Jahn, 1995; Xu et al., 2001). Evidence for plume origin includes short duration of volcanism, high content of MgO and high potential mantle temperature (~1500 °C). A surrounding region experienced uplift of more than 1 km shortly before the emplacement of the Emeishan basalts, which is indicative of a thermal upwelling (He et al., 2003).

Piercing points of stations CHTO and KMI are beneath the Yangtze craton, close to the Emeishan traps. It should be taken into account, that the Emeishan basalts were subjected to erosion, and the current estimate of their surface exposure is a minimum (He et al., 2003). The piercing points of the two other stations (ENH and XAN) are at a large (more than 500 km) distance from the traps. The absence of detectable signals from the 350-km discontinuity in the data of the distant stations suggests that the low-S-velocity layer over the 410-km discontinuity is indeed related to the traps, as in the case of the Siberian traps.

3.5. The Arabian plate, station RAYN

Receiver functions for station RAYN (Fig. 6e) contain a very clear Sp phase from the 350-km discontinuity: the amplitude of this signal is 5 times the RMS noise amplitude. The signal is focused at a differential slowness of 0.2 s/°, 0.4 s/° less than the standard value. The deviation could be caused by a tilt of the 350-km discontinuity of around 2°, dipping to the west. The average back azimuth of the related seismic events is close to 90°, and the corresponding piercing point is beneath the eastern margin of the Arabian plate (for a detailed map see Vinnik et al., 2003), close to the Arabian sea and Persian Gulf. Previously a lower-quality signal from the 350-km discontinuity was detected in S receiver functions for a group of stations located mostly to the west of station RAYN (Vinnik et al., 2003). A negative-polarity signal is detected at a time of around −30 s at a slowness of 0.2 s/°. This is the Sp phase from the Lehmann discontinuity at a depth of about 200 km.

The Arabian plate is of Proterozoic age. Its western region experienced magmatic activity in the last 14 Myr (Camp and Robol, 1992). The earlier phase of magmatism (30–20 Myr) in western Arabia was roughly contemporaneous with opening of the Red sea and the Gulf of Aden rifts (Mohr and Zanettin, 1988). S velocity in upper mantle of the western Arabian plate is anomalously low (Knox et al., 1998). Available tomographic maps do not show any extension of this mantle anomaly to the east, but previously the low S velocity layer atop the 410-km discontinuity was ascribed to the Afro-Arabian hotspot (Vinnik et al., 2003). However, the signal that we observe at station RAYN is large in comparison with that at the group of stations mostly to the west of RAYN. This trend suggests that the effect may increase from the west to the east and may indicate that the anomaly is related not to the Afro-Arabian hotspot, but to the large low-velocity body in the mantle transition zone beneath the Arabian sea, to the east of the Arabian plate. This body is clearly imaged in global tomographic maps (e.g., Ritsema and van Heijst, 2000; Megnin and Romanowicz, 2000).

3.6. North Africa, station TAM

Receiver functions for station TAM in northern Africa (Fig. 6f) in back azimuths around 250° contain Sp phases with negative polarity from the Moho, Lehmann, 410-km and 660-km discontinuities. Detection of the signal from the 660-km discontinuity is facilitated by the presence of many recordings at large (more than 90°) epicentral distances in this data set. The signal from the 410-km discontinuity is followed by the Sp phase from the 350-km discontinuity at a slowness of 1.2 s/°, much larger than the standard value. The amplitude of this signal (0.022) is more than 4 times the RMS noise amplitude. The deviations of differential slowness of the other signals from the standard values are smaller. This suggests that the slowness anomaly of the 350-km phase is caused mainly by a tilt of that discontinuity, dipping to the west at an angle of about 3°.

North Africa is known as a region of widespread Cenozoic volcanism (Hoggar, Tibesti, Darfur and others). Geochemical signatures of the extrusives suggest a shallow mantle upwelling, presumably originating from a depth of less than 400 km (Pik et al., 2006). The seismograph station TAM is in the center of the Hoggar swell, corresponding to the Hoggar hotspot (Fig. 2e). The age of the volcanism is from late Mesozoic to the Quaternary. S velocity in the upper mantle is lower than the usual velocity beneath Precambrian cratons but higher than in thermally active regions (Ayadi et al., 2000), and at present the Hoggar hotspot is practically extinct. The piercing point of the Sp phase at a depth of 350 km is beneath the West-African craton of Archean age. Owing to African plate motion to the NNE, a plume related to the Hoggar hotspot may now be located 400 km to the WSW of TAM (Ait Hamou and Dautria, 1994), practically at the piercing point. The low velocity atop the 410-km discontinuity might be related to this plume.

3.7. East Antarctica, stations DRV, SPA and SBA

In Antarctica, the available data are from stations DRV, SPA and SBA (Fig. 2f). The recordings are either from events in southeastern Asia and the west Pacific (SPA and SBA) or in south America (DRV). The receiver functions of station DRV (Fig. 6g) contain a clear Sp phase from the 350-km discontinuity with an amplitude more than 4 times the RMS noise amplitude. The signal is focused at a differential slowness of 0.8 s/°, little different from the standard value.

In the receiver functions of station SPA (Fig. 6h), there is a positive phase, large at all traces from 0.8 s/° to −0.4 s/°. The largest amplitude (at 0.6 s/°) of the signal, which we interpret as the Sp phase from the 350-km discontinuity, is more than 4 times the RMS noise amplitude. The relatively low sensitivity of this data set to differential slowness is caused mainly by the narrow distance range of the available seismic events. At a time of about −30 s there is an arrival corresponding to the Lehmann discontinuity at a depth of about 200 km. The differential slowness of this signal (−0.2 s/°) is similar the standard value for this depth. Constructive interference between a side-lobe of this phase and the Sp phase from the 350-km discontinuity could explain the large amplitude and long period at a time of about −40 s at a differential slowness of about 0 s/°.

In the receiver functions of station SBA (Fig. 7d) the signal from the 350-km discontinuity is practically missing.

East Antarctica (Fig. 2f) is a stable Precambrian plate: crustal rocks found at the perimeter of East Antarctica are of Archean and Proterozoic age. The margin of East Antarctica near its border with West Antarctica is formed by the Trans-Antarctic mountains, which are interpreted as a flexural uplift that started in the early Cenozoic (ten Brink et al., 1997). In east Antarctica, along the border with the west Antarctica there is a narrow band of Ferrar flood basalts, dated at 177 Myr (Heinmann et al., 1995).

West Antarctica was accreted during the Paleozoic (Dalziel and Elliot, 1982). Its western margin is occupied by the West Antarctic rift system (Wörner, 1999). The volcanic rocks associated with the rift were

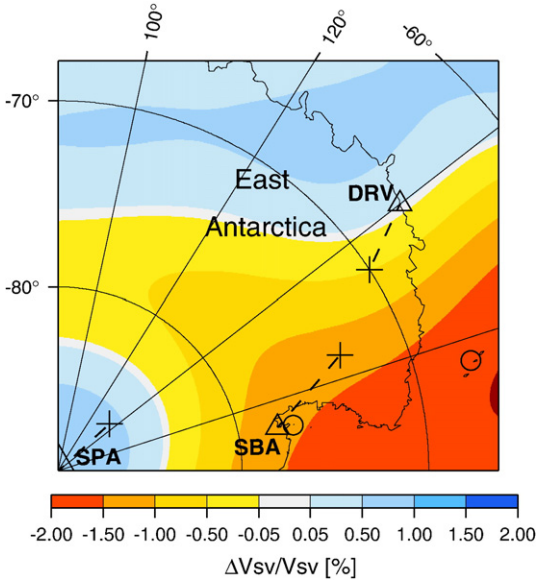

Fig. 8. S velocity at a depth of 500 km beneath Antarctica (adopted from Megnin and Romanowicz, 2000). Stations, piercing points and hotspots are taken from Fig. 2f.

deposited in the last 30 Myr. Origins of the volcanism and its possible relation to mantle plumes are debated, but the study, based on the surface wave higher modes reveals beneath West Antarctica vertical low velocity structures extending from the asthenosphere to the mantle transition zone (Sieminski et al., 2003). This presents a strong argument in favor of several plumes. The low velocity atop the 410-km discontinuity beneath station SPA is very likely related to these plumes.

As shown by global tomographic maps (e.g., Ritsema and van Heijst, 2000; Megnin and Romanowicz, 2000), station DRV is located near a large low-velocity anomaly in the mantle transition zone (Fig. 8). P receiver functions from this station reveal thinning of the mantle transition zone, one of the largest found with this technique (Chevrot et al., 1999). Thinning (shortening of the depth interval between the 410-km and 660-km discontinuities) is indicative of anomalously high temperature, and the low-velocity zone atop the 410-km discontinuity in the vicinity of this station is very likely related to a plume-like structure in the mantle.

4. Discussion

We present evidence for a positive Sp phase and the related negative 350-km discontinuity at a number of locations in Asia, Africa and Antarctica. Estimates of the signal/noise ratio indicate that the signal detection is robust. One could suspect, however, that the positive phase still is an artifact. The anelastic attenuation of the S410p phase is weaker than of the parent S wave. Then the S410p waveform may differ from the S waveform, and an anomalously large S410p side lobe could be mistaken for the S350p phase. We tested this possibility with synthetic seismograms by adopting a very low quality factor Q for the S wave (Q=80) in the upper mantle and indefinitely high Q for the P wave. Then the S410p amplitude at the periods of about 10 s is about 40% larger than in the perfectly elastic mantle, whereas the ratio between the side lobe and the main lobe is practically the same as in the S wave. Moreover, similar S350p phases are observed in the low-attenuation regions (Kaapvaal and Siberian cratons) and the high-attenuation regions of Cenozoic volcanism. Finally, the negative 350-km discontinuity beneath northeast China, very similar to that in our data, was found using very different data and techniques (Revenaugh and Sipkin, 1994).

The exact depth of the 350-km discontinuity can be inferred from the delay of the S350p phase relative to S410p (last column of Table 1). It varies between approximately 360 km (station RAYN) and 320 km (station SPA). Beneath the 350-km discontinuity S velocity is lowered by 0.15–0.2 km/s. In most cases, the 350-km discontinuity is found beneath Precambrian platforms (Kaapvaal, Siberian, West-African, Yangtze, Sino-Korean, Arabian and East Antarctica), in association with Mesozoic and Cenozoic large igneous provinces (LIPs), mantle plumes, and hotspots. For every region taken separately from the others, a few explanations for the 350-km discontinuity might be found. However, if one explanation should be suggested for all regions, the relationship between the 350-km discontinuity and Mesozoic and Cenozoic volcanism is the most plausible, if not unique.

In some studies the low-velocity layer atop the 410-km discontinuity is attributed to subduction (Revenaugh and Sipkin, 1994; Song et al., 2004; Nolet and Zielhuis, 1994). According to Revenaugh and Sipkin (1994) the low velocity beneath north-eastern China is caused by dehydration of subducting lithospheric slabs about 1000 km to the east of the study region and migration of dense melt atop the 410-km discontinuity. However, the resolution of seismic data is too low to recognize a continuous layer of melt connecting the subduction zone with the continental interior. Moreover, our analysis suggests that the low velocity in this region is related to the surface exposures of Cenozoic basalts (Fig. 2c). Cenozoic basalts are widespread in central and east Asia, and their origin is likely caused by plumes (e.g., Deng et al., 2004; Kovalenko et al., 1995; Barry and Kent, 1998). No evidence for the 350-km discontinuity is

found beneath the western Sino-Korean craton, outside the volcanic region (station LZH). In Russia, adjacent to north-eastern China, at the same or smaller distances from the nearest subduction zone, a similar magmatic activity is absent, and there is no evidence for the low velocity layer (Vinnik et al., 1996a). Observations of the low velocity in the north-west USA were explained in a similar way by dehydration of the subducted Farallon plate (Song et al., 2004). However, a simple comparison of these observations with geology (Fig. 9) demonstrates that the low velocity is likely associated with Columbia river flood basalts, a classic plume ca. 15 Myr old (Camp and Ross, 2004).

In our data set there are a few observations within or near LIPs in old continental platforms but without evidence for the 350-km discontinuity. Station LBTB of this group samples the upper mantle of Zimbabwe craton, neighboring to the Karoo traps. Station BOSA where the Sp phase from the 350-km discontinuity is very large (Vinnik and Farra, 2006) and LBTB are at a distance of about 400 km. This distance can be viewed as a rough estimate of the lateral extent of the 350-km discontinuity in south Africa. Similarly, lateral variability of the 350-km discontinuity may explain the failure to detect the signal from the 350-km discontinuity at station SBA in Antarctica and at a few other stations. The Sp phase from the 350-km discontinuity may become invisible if this discontinuity is gradational with a thickness of about 70 km or more. Stations PTGA and MPG in south America are in the area belonging to the Central Atlantic Magmatic Province (CAMP). The CAMP traps erupted at

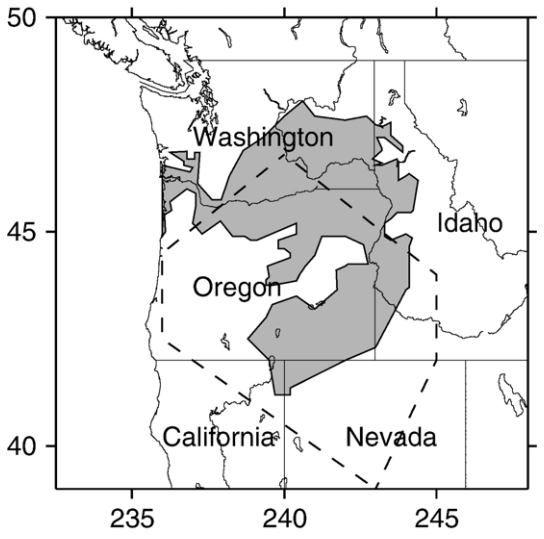

Fig. 9. Map of the northwest USA with flood basalts (shaded) (Camp and Ross, 2004) and the area of low S velocity atop the 410-km discontinuity (Song et al., 2004) (dash line).

200 Myr in a close association with the Central Atlantic breakup (Marzoli et al., 1999). Station ATD (Vinnik et al., 2004a) and two neighboring temporary stations (Vinnik and Farra, 2006) located in the Afar hot spot sample the upper mantle in the vicinity of the Gulf of Aden rift. It is possible that the breakup of the continental lithosphere prevents development of the low-velocity layer in the neighboring area. Moreover, a deep-mantle plume origin of the CAMP magmatism is disputed (McHone, 2000).

There is a large group of stations (Fig. 1) in the old continental regions where the 350-km discontinuity is missing and there is no evidence for either Cenozoic or Mesozoic hotspots and plumes: OBN, KIEV, LVZ, KONO (Europe); YAK, TIXI, BRVK, HYB, NIL, LZH, ENH, XAN, several stations of GHENGYZ network (Asia); BNG (Africa), NWAO (Australia), FFC, FRB, SCHQ, YKW3, SSPA, CCM, several stations of MOMA array (North America). The 350-km discontinuity is also missing in the Himalaya (station NIL) and Tibet (station LSA), where enormous volume of the Tethys lithosphere has been subducted in the Mesozoic.

To summarize, the 350-km discontinuity, if it is detected, is usually found in the old continental regions in association with LIPs, plumes and hot spots, but it was not detected in some regions of this category.

The Karoo, Emeishan and Siberia traps are 180–260 Myr old. The plates have moved since the Mesozoic magmatic events to new locations separated from the old ones by at least 2000 km. For example, Emeishan traps were erupted at the equator (Davaille et al., 2005), whereas their present location is at a latitude of about 25° N. The Karoo traps erupted to the southwest of their present-day location, near the current Bouvet hotspot. The detections of the 350-km discontinuity beneath old traps in spite of plate motions suggest that it moved coherently with the lithosphere (Vinnik and Farra, 2002). This is consistent with the concept of the tectosphere (Jordan, 1975).

Some authors have reported observations of a positive discontinuity (the “X” discontinuity) near 300-km depth (Revenaugh and Jordan, 1991; Deuss and Woodhouse, 2004). In our data there is one observation of this discontinuity (station LZH, Fig. 7a). Stratification of the mantle is laterally heterogeneous, and, like the negative 350-km discontinuity, the “X” discontinuity may be present in some regions but absent in the others.

Origin of the low velocity is hard to explain by elevated temperature alone: the temperature appears to be too high for the plumes 200 Myr old, and the assumption of high temperature alone cannot explain why the effect is localized in a narrow depth range. More likely, this layer is different in composition from the rest of the upper mantle. A likely reason for the low velocity

is high solubility of water in wadsleyite in the mantle transition zone relative to olivine in the overlying mantle (up to about 2 wt.% below the 410-km discontinuity versus .2 wt.% over it) (Hirschmann et al., 2005). Then, if the water content in the MTZ is close to saturation, mantle upwelling across the 410-km discontinuity leads to dehydration and melting of the rock on the upper side of the discontinuity (Kawamoto et al., 1996). The melt may be gravitationally trapped at that depth and spread laterally.

Dehydration and melting over the 410-km discontinuity and the related water-filter hypothesis (Bercovici and Karato, 2003) may explain chemical differences between mid-ocean-ridge basalts and ocean-island basalt by assuming that dehydration and melting do not operate in the plumes: high plume temperature prevents dehydration at a depth of 410 km and generation of melts, because water solubility in olivine at high temperature is close to that in wadsleyite (Demouchy et al., 2005). The hypothesis predicts that the low-S-velocity layer ca. 10-km thick is present almost everywhere atop the 410-km discontinuity but absent in the plumes. The resolution of our method is too low for detecting the 10-km layer. Otherwise our results are very different from the predicted: the low-S-velocity layer ~60-km thick is associated with plumes, and is not found elsewhere. Plumes might be colder than assumed by the water-filter model, or the layer is of a different origin, for example, caused by carbonate with a low melting temperature (Presnall and Gudfinnsson, 2005). Moreover, the whole concept of plumes is disputed (Anderson, 2005). If the water-filter hypothesis still is correct in predicting a thin (~10 km) low-velocity (and low-viscosity) layer atop the 410-km discontinuity almost everywhere, this would result in a decoupling between the mantle over and beneath the 410-km discontinuity. This might explain the coherent motion of the lithosphere and the underlying mantle up to a depth of ~400 km, as suggested by some of our observations.

Acknowledgements

This study was supported by the Russian Fund for Basic Research, grants 04-05-64634 and 07-05-00315. The authors appreciate constructive comments from two anonymous reviewers. Gillian Foulger made thoughtful comments and helped to improve our English. Seismic recordings were obtained from the IRIS DMC.

References

Anderson, D.L., 2005. Scoring hotspots: the plume and plate paradigms. In: Foulger, G.R., Natland, J.H., Presnall, D.C., Anderson, D.L. (Eds.), Plates, plumes, and paradigms: Geological Society of America Special Paper, 388, pp. 31–54.

Ait Hamou, F., Dautria, J.M., 1994. Le magmatisme Cenozoique du Hoggar: une synthese des donnees disponibles. Mise au point sur l'hypothese d'un point chaud. Bull. Serv. Carte Geol. Alger. 5 (1), 49–68.

Ayadi, A., Dorbath, C., Lesquer, A., Bezzeghoud, M., 2000. Crustal and upper mantle velocity structure of the Hoggar swell (Central Sahara, Algeria). Phys. Earth Planet. Inter. 118, 111–123.

Barry, T.L., Kent, R.W., 1998. Cenozoic magmatism in Mongolia and the origin of the central and east Asian basalts. In: Flowers et al. (Ed.), Mantle dynamics and plate interactions in east Asia. AGU Geodynamics Series, 27, pp. 347–364.

Bercovici, D., Karato, S.-I., 2003. Whole-mantle convection and the transition-zone filter. Nature 425, 39–44.

Berkhout, A.J., 1977. Least square inverse filtering and wavelet decomposition. Geophysics 42, 1369–1383.

Chang, S.I., Jahn, B.M., 1995. Plume-lithospherical interaction in generation of the Emeishan flood basalts at the Permian–Triassic boundary. Geology 23, 889–892.

Camp, V.E., Robol, M.J., 1992. Upwelling asthenosphere beneath western Arabia and its regional implications. J. Geophys. Res. 97, 15 255–15 271.

Camp, V.E., Ross, M.E., 2004. Mantle dynamics and genesis of mafic magmatism in the intermontane Pacific Northwest. J. Geophys. Res. 109, B08204. doi:10.1029/2003JB002838.

Chevrot, S., Vinnik, L., Montagner, J.-P., 1999. Global scale analysis of the mantle Pds phases. J. Geophys. Res. 104, 20203–20219.

Dalziel, I.W.D., Elliot, D.H., 1982. West Antarctica: problem child of Gondwanaland. Tectonics 1, 3–19.

Davaille, A., Stutzmann, E., Silveira, G., Besse, J., Courtillot, V., 2005. Convective pattern under the Indo-Atlantic "box". Earth Planet. Sci. Lett. 239, 233–252.

Demouchy, S.E., Deloule, E., Frost, D.J., Keppler, H., 2005. Pressure and temperature dependence of water solubility in Fe-free wadsleyite. Am. Mineral. 90, 1084–1091.

Deng, J.F., Mo, X.X., Zhao, H.L., Wu, Z.X., Su, S.G., 2004. A new model for the dynamic evolution of Chinese Lithosphere: 'continental roots-plume tectonics'. Earth-Sci. Rev. 65, 223–275.

Deuss, A., Woodhouse, J.H., 2004. The nature of the Lehmann discontinuity from its seismological Clapeyron slopes. Earth Planet. Sci. Lett. 225 (3-4), 295–304.

Duncan, R.A., Richards, M.A., 1991. Hotspots, mantle plumes, flood basalts, and true polar wander. Rev. Geophys. 29, 31–50.

Efron, B., Tibshirani, R., 1991. Statistical data analysis in the computer age. Science 253, 390–395.

Farra, V., Vinnik, L., 2000. Upper mantle stratification by P and S receiver functions. Geophys. J. Int. 141, 699–712.

Griffin, W.L., Zhang, A., O'Reilly, S.Y., Ryan, C.G., 1998. Phanerozoic evolution of the lithosphere beneath the Sino-Korean Craton. In: Flower, M., Chung, S.L., Lo, C.H., Lee, T.Y. (Eds.), Mantle Dynamics and Plate Interactions in East Asia, Geodynamics Series 27. Amer. Geophys. Union, Washington D.C, pp. 107–126.

He, B., Xu, Y.-G., Chung, S.-L., Xiao, L., Wang, Y., 2003. Sedimentary evidence for a rapid, kilometer-scale crustal doming prior to the eruption of the Emeishan flood basalts. Earth Planet. Sci. Lett. 213, 391–405.

Heinmann, A., Fleming, T.H., Elliot, D.H., Foland, K.A., 1995. A short interval of Jurassic continental flood basalt volcanism in Antarctica as demonstrated by $^{40}Ar/^{39}Ar$ geochronology. Earth Planet. Sci. Lett. 121, 19–41.

Hirschmann, M.M., Abaud, C., Withers, A.C., 2005. Storage capacity of H_2O in nominally anhydrous minerals in the upper mantle. Earth Planet. Sci. Lett. 236, 167–181.

Jordan, T., 1975. The continental tectosphere. Rev. Geophys. 13, 1–12.

Kawamoto, T., Hervig, R., Holloway, J., 1996. Experimental evidence for a hydrous transition zone in the early earth's mantle. Earth Planet. Sci. Lett. 142, 587–592.

Kennett, L.N., Engdahl, E.R., 1991. Traveltimes for global earthquake location and phase identification. Geophys. J. Int. 105, 429–465.

Knox, R.B., Nyblade, A.A., Langston, C.A., 1998. Upper mantle S velocities beneath Afar and western Saudi Arabia from Rayleigh wave dispersion. Geophys. Res. Lett. 25, 4233–4236.

Kovalenko, V.I., Yarmolyuk, V.V., Bogatikov, O.A., 1995. Magmatism, Geodynamics and Metallogeny of Central Asia. Mico, Moscow.

Marzoli, A., Renne, P.R., Piccirillo, E.M.E.M., Ernesto, M., Bellieni, G., de Min, A., 1999. Extensive 200-Million-Year-old continental flood basalts of the Central Atlantic Magmatic Province. Science 284, 616–618.

McHone, J.G., 2000. Non-plume magmatism and tectonics during the opening of the central Atlantic ocean. Tectonophysics 316, 287–296.

Megnin, C., Romanowicz, B., 2000. The three-dimensional shear velocity structure of the mantle from the inversion of body, surface and higher-mode waveforms. Geophys. J. Int. 143, 709–728.

Mohr, P.A., Zanettin, B., 1988. The Ethiopian flood basalt province. In: Macdughall, D.J. (Ed.), Continental flood basalts. Nouvell. Mass, Kluwer Acad., pp. 63–110.

Nolet, G., Zielhuis, A., 1994. Low S velocities under the Tornquist–Teisseyre zone: evidence for water injection into the transition zone by subduction. J. Geophys. Res. 99, 15 813–15 820.

Oreshin, S., Vinnik, L., Peregoudov, D., Roecker, S., 2002. Lithosphere and asthenosphere of the Tien Shan imaged by S receiver functions. Geophys. Res. Lett. 29 (8). doi:10.1029/2001GL014441.

Pik, R., Marty, B., Hilton, D.R., 2006. How many plumes in Africa? The geochemical point of view. Chem. Geol. 226, 110–114.

Presnall, D.C., Gudfinnsson, G.H., 2005. Carbonate-rich melts in the oceanic low-velocity zone and deep mantle. In: Foulger, G.R., Natland, J.H., Presnall, D.C., Anderson, D.L. (Eds.), Plates, plumes, and paradigms: Geological Society of America Special Paper, 388, pp. 207–216.

Reichow, M.K., Sauders, A.D., Weight, R.V., Pringl, M.S., Al'mukhamedov, A.I., Medvedev, A.Ya., Kirda, N.P., 2002. $^{40}Ar/^{39}Ar$ dates from the west Siberian basin: Siberian flood basalt province doublet. Science 296, 1846–1849.

Revenaugh, J., Jordan, T.H., 1991. Mantle layering from ScS reverberations, 3, The upper mantle. J. Geophys. Res. 96, 19 781–19 810.

Revenaugh, J., Sipkin, S., 1994. Seismic evidence for silicate melt atop the 410-km discontinuity. Nature 369, 474–476.

Ritsema, J., van Heijst, H.J., 2000. Seismic imaging of structural heterogeneity in Earth's mantle: evidence for large-scale mantle flow. Sci. Prog. 83, 243–259.

Sengor, A.M.C., Natal'in, B.A., Burtman, V.S., 1993. Evolution of the Altaid tectonic collage and Paleozoic crustal growth in Eurasia. Nature 364, 299–307.

Sieminski, A., Debayle, E., Leveque, J.-J., 2003. Seismic evidence for deep low-velocity anomalies in the transition zone beneath West Antarctica. Earth Planet. Sci. Lett. 216, 645–661.

Song, T.-R.A., Helmberger, D.V., Grand, S.P., 2004. Low-velocity zone atop the 410-km seismic discontinuity in the northwestern United States. Nature 427, 530–533.

ten Brink, U.S., Hackney, R.I., Bannister, S., Stern, T.A., Makovsky, Y., 1997. Uplift of the transantarctic mountains and the bedrock beneath the east Antarctic ice sheet. J. Geophys. Res. 102, 27 603–27 621.

Vinnik, L., Kosarev, G., Petersen, N., 1996a. Mantle transition zone beneath Eurasia. Geophys. Res. Lett. 23, 1485–1488.

Vinnik, L.P., Green, R.W.E., Nicolaysen, L.O., 1996b. Seismic constraints on dynamics of the mantle of the Kaapvaal craton. Phys. Earth Planet. Inter. 95, 139–151.

Vinnik, L.P., Kumar, M.R., Kind, R., Farra, V., 2003. Super-deep low-velocity layer beneath the Arabian plate. Geophys. Res. Lett. 30, 1415. doi:10.1029/2002GL016590.

Vinnik, L., Farra, V., Kind, R., 2004a. Deep structure of the Afro-Arabian hotspot by S receiver functions. Geophys. Res. Lett. 31, L11608. doi:10.1029/2004GL019574.

Vinnik, L.P., Reigber, Ch., Aleshin, I.M., Kosarev, G.L., Kaban, M.K., Oreshin, S.I., Roecker, S., 2004b. Receiver function tomography of the central Tien Shan. Earth Planet. Sci. Lett. 225, 131–146.

Vinnik, L., Kurnik, E., Farra, V., 2005a. Lehmann discontinuity beneath North America: no role for seismic anisotropy. Geophys. Res. Lett. 32, L09306. doi:1029/2004GL022333.

Vinnik, L.P., Foulger, G.R, Du, Z., 2005b. Seismic boundaries in the mantle beneath Iceland: a new constraint on temperature. Geophys. J. Int. 160, 533–538.

Vinnik, L., Farra, V., 2006. S velocity reversal in the mantle transition zone. Geophys. Res. Lett. 33, L18316. doi:10.1029/2006GL027120.

Vinnik, L., Farra, V., 2002. Subcratonic low-velocity layer and flood basalts. Geophys. Res. Lett. 29, 1049. doi:10.1029/2001GL014064.

Wörner, G., 1999. Lithospheric dynamics and mantle sources of alkaline magmatism of the Cenozoic West Antarctic Rift System. Glob. Planet. Change 23, 61–77.

Xu, Y.G., Chung, S.L., Jahn, B.M., Wu, G.Y., 2001. Petrologic and geochemical constraints on the petrogenesis of Permian–Triassic Emeishan flood basalts in southern China. Lithos 58, 145–168.

Zhang, Z.-H.M., Liou, J.G., Coleman, R.G., 1984. An outline of the plate tectonics of China. Geol. Soc. Amer. Bull. 95, 295–312.

Zolutkhin, V.V., Al'mukhamedov, A.I., 1988. Traps of the Siberian platform. In: Macdughall, D.J. (Ed.), Continental flood basalts. Nouvell. Mass., Kluwer Acad., pp. 273–310.

Zonenshain, L.P., Korinevsky, L.P., Kazmin, V.G., Pechersky, D.M., Khain, V.V., Matveenkov, V.V., 1984. Plate tectonic model of the south Urals development. Tectonophysics 109, 95–135.